Infrared Physics and Technology 94 (2018) 23–31

Contents lists available at ScienceDirect

Infrared Physics & Technology

journal homepage: www.elsevier.com/locate/infrared

Regular article

# A design of multi-mode excitation source for optical thermography nondestructive sensing

Yuyu Zhu[a], Bin Gao[a,*], Shichun Wu[a], Yangzhen Zhang[c], Meiling Wang[a], W.L. Woo[b], Yongbo Liao[a]

[a] School of Automation Engineering, University of Electronic Science and Technology of China, Chengdu, China
[b] School of Electrical and Electronic Engineering, Newcastle University, England, United Kingdom
[c] University of Michigan-Shanghai Jiao Tong University Joint Institute, China

ARTICLE INFO

*Keywords:*
Non-destructive testing
Optical thermography
Excitation source

ABSTRACT

Optical thermography is an important non-destructive testing (NDT) method which has been widely used in the fields of modern aerospace, renewable energy, nuclear industry, etc. The excitation source is a crucial device for the optical thermography system whose performance has a decisive effect on the detection results. Previous thermography NDT studies mainly focused on the physical mechanism, applications and signal processing algorithms. However, the design of the excitation source is rarely discussed. Due to the wide frequency range as well as the high power excitation requirements, it is a challenging task to develop a multi-mode excitation source for thermography NDT. This paper presents a novel design of the excitation source with a structure topology that combines the circuit with low frequency sinusoidal generation and a chopper circuit. It intimately satisfies the requirements of multiple-mode excitation for optical thermography. These include pulsed thermography (PT), lock-in thermography (LT), step heating thermography (ST), pulsed phase thermography (PPT), frequency modulated thermal wave imaging (FMTWI) and barker coded thermal wave imaging (BCTWI). The proposed topology, operating principle and the design procedure of the circuit have been investigated in details. A 2 kW prototype with a frequency range of 0.01 Hz–100 kHz has also been implemented. Validation of the proposed method has been undertaken to detect inner defects of both on a composite sample and a lead-steel sample with bonded structure.

## 1. Introduction

The excitation source has been widely used in the sensing and detection fields as a part of the system, such as laser detection [1], electromagnetic thermography testing [2], ultrasound inspection [3], and plasma detection [4]. The excitation sources can be implemented by utilizing the power electronics technology, such as AC-DC, DC-AC, DC-DC and AC-AC conversion. However, researchers in this field mainly concern in the performance index of power conversion, such as efficiency, power factor, ripple, and power density. This research directions include design topologies [5,6], control strategies [7–9] and new power electronic components [10,11]. Therefore, it is necessary to hybrid the requirements of the sensing and detection with the power electronics technology to design a functional excitation source for the specific diagnosis system.

Active infrared thermography (AIT) was developed to provide more accurate information by considering the amount of thermal radiation and heat transfer. Due to the different external excitation source in AIT, it can be divided into inductive thermography, optical thermography, vibro-thermograph, etc. [12]. Optical thermography has gained increasing attention because of its non-destructive imaging characteristics with high precision and sensitivity [13]. It has been applied to the defect inspection and evaluation of composite materials such as glass fiber reinforced polymers (GFRP), carbon fiber reinforced polymers (CFRP) and adhesive bonds [14–17]. Depending on the different heating excitation mode, it can be divided into pulsed thermography (PT), lock-in thermography (LT), step heating thermography (ST), pulsed phase thermography (PPT), frequency modulated thermal wave imaging (FMTWI), barker coded thermal wave imaging (BCTWI), etc. [24–31].

In PT, the sample surface is stimulated by a short pulse with a high power light lamp. The thermal wave propagates from the sample surface into the inner part through diffusion. The resultant sequence of infrared images has potential to indicate defects in the sample at different depths [18–21]. The method apart from requiring high power heat sources, has additional drawback of being sensitive to surface

* Corresponding author.
*E-mail address:* bin_gao@uestc.edu.cn (B. Gao).

https://doi.org/10.1016/j.infrared.2018.08.023
Received 4 May 2018; Received in revised form 20 August 2018; Accepted 27 August 2018
Available online 30 August 2018
1350-4495/ © 2018 Elsevier B.V. All rights reserved.

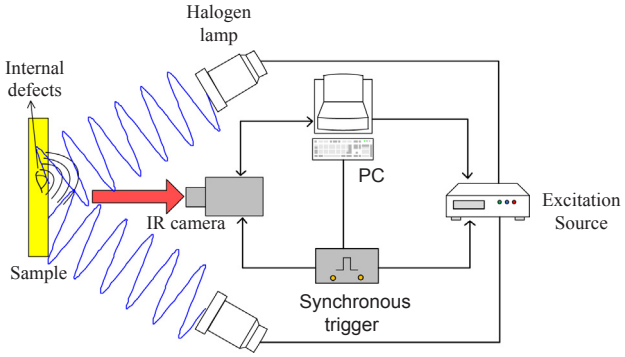


**Fig. 1.** Diagram of the optical thermography.

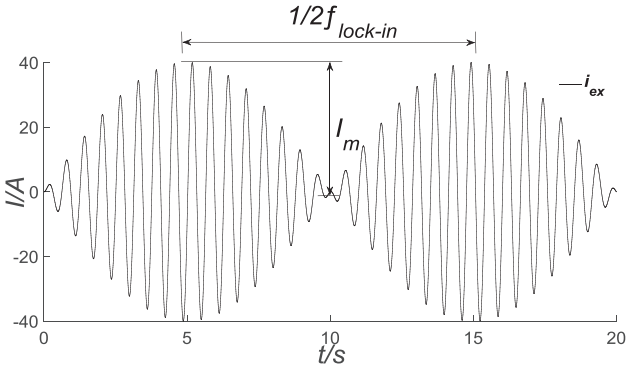


**Fig. 2.** Profile of the lock-in excitation current.

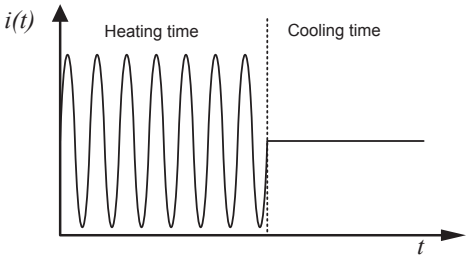


**Fig. 3.** Profile of the pulsed excitation current.

inhomogeneities. In LT, the sample is heated using a mono-frequency sinusoidal thermal excitation. The magnitude of the periodic temperature change at the surface and its phase with respect to the applied modulated heating is extracted by using post-processing algorithms for defect detection [22]. This method has advantages of better signal-to-noise (S/N) ratio and adjustable depth range for inner defect visualization. However, it demands a selection of a suitable frequency to avoid the blind frequencies and the repetitive experiments are required to resolve the defects location at different depths [23]. ST based on temporal temperature analysis caused by step excitation in time domain is similar to PT in heating excitation mode which has longer heating time. PPT is same to PT in heating excitation mode, where, an analysis is carried out by phase mode which has the merits of phase images obtained with LT [24]. In FMTWI, the sample is heated by using excitation source with a limited range of frequencies. This method attempts to overcome the drawbacks of LT [25–27]. In BCTWI, the sample is heated using a binary coded thermal excitation. This excitation method combines with correlation processing which can provides better detection capabilities and better depth resolution [28–30]. Those methods usually use flash lamps or halogen lamps as a heating source which are excited by an excitation source such as power amplifier with signal generator.

Previous studies mainly have been focused on the principles, various applications and signal processing algorithms [23–34] for optical thermography in NDT. However, the design of the excitation source is rarely discussed. Due to the requirements of wide frequency range (typically 0.01 Hz to several hundred kHz) and high power (typically hundreds of W to several kW), the design and the developing of the particular multi-modality excitation source for thermography is highly challenging. One promising approach is to utilize a high voltage linear amplifier, but the downside is its restriction by the gain bandwidth product (GBP) which can lead to a low efficiency [35]. In recent years, digital control power converters have been described as be able to offer a high capability to efficiently manage electrical energy as they are widely applied in industrial applications, electric traction systems, renewable energy systems, distributed generation, and automotive [36]. Thus, this paper proposes a structural design topology of a multi-mode excitation source with high performance under the framework of a digital control strategy. This paper presents the design of an excitation source with a maximum output power of 2.0 kW and a wider frequency band ranging from 0.01 Hz to 100 kHz which is used to drive the halogen lamps. The proposed topology, operating principle, and the design procedure of the circuit have been investigated. In addition, experimental validations been conducted to verify the proposed methodology.

The paper is organized as follows: Section 2 discusses the optical thermography characteristics, Section 3 describes the proposed solution and topology. Section 4 describes operating principle; Section 5 presents the experimental results and discussion. Finally, Section 6 concludes the work.

## 2. Optical thermography sensing

Fig. 1 shows the diagram of the optical thermography system. Halogen lamps or flash lamps are driven from pre-set current which is generated by excitation source. The incident light generates the heat on the sample and the heat diffuses in time. Defects such as cracks, debonds, delamination alters the heat diffusion and the progress is recorded by infrared (IR) camera. A synchronous trigger receives the “start” command from the PC and then triggers the IR camera and the excitation source to work synchronously. According to the different pre-

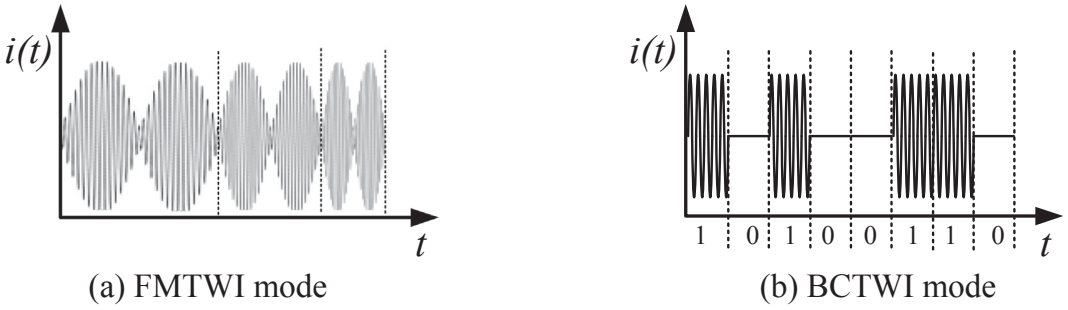


**Fig. 4.** Profile of the (a) FMTWI and (b) BCTWI excitation current.

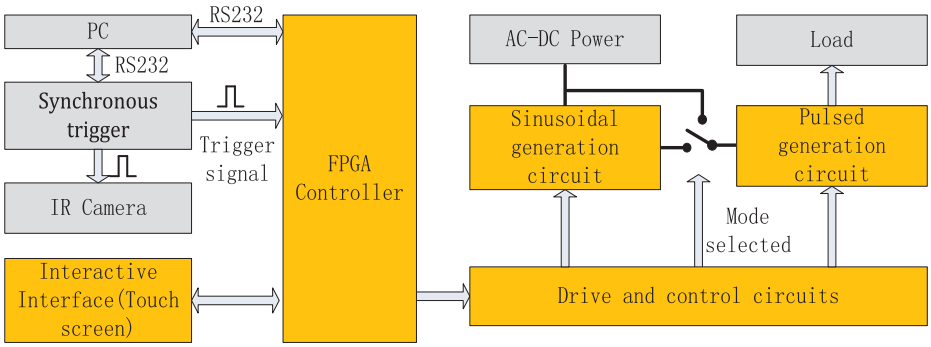


**Fig. 5.** Block diagram of the designed excitation source.

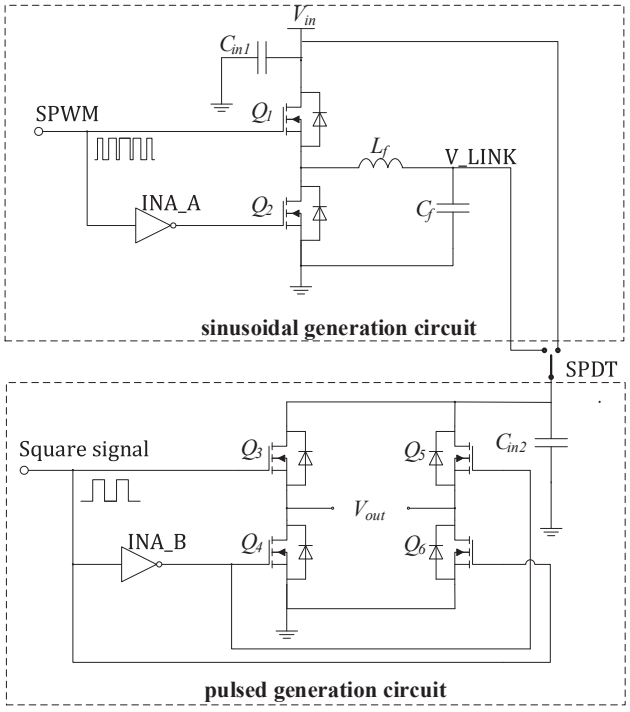


**Fig. 6.** Proposed design topology.

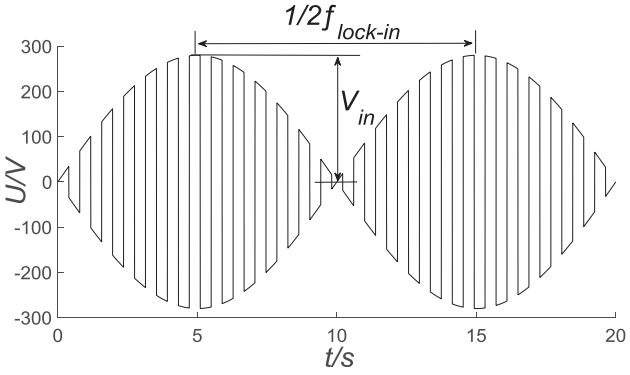


**Fig. 7.** Output signal waveform in LT mode.

set excitation current, it can work in LT mode, PT, ST, PPT mode, FMTWI mode and BCTWI mode.

In LT mode, the pre-set current is amplitude-modulated current $i_{ex}$ which is formed by combining a low-frequency sinusoidal signal with a high-frequency signal which can be expressed as (1) and its profile shows as Fig. 2.

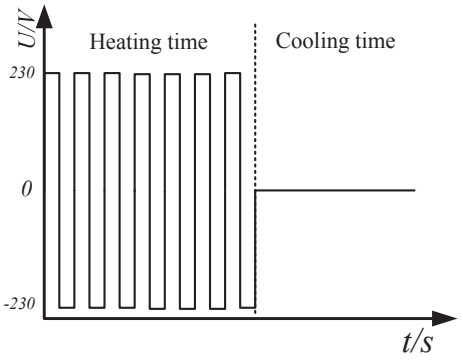


**Fig. 8.** Output signal waveform in PT mode.

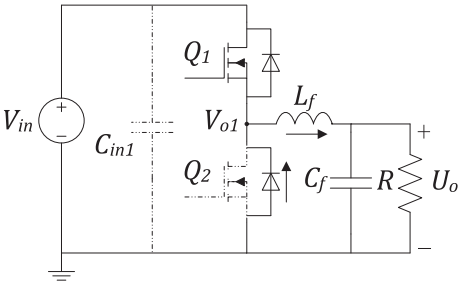


**Fig. 9.** Sinusoidal generation circuit.

$$i_{ex} = I_m \cdot \sin(2\pi f_{lock} t) \cdot \sin(2\pi f_{carr} t) \quad (1)$$

where $I_m$ is the maximum of the amplitude. $f_{\text{lock}}$ and $f_{\text{carr}}$ are lock-in frequency and carrier frequency, respectively.

According to the theory of thermal wave, the probing depth of defects depends on the length of the thermal diffusion which can be present as:

$$\mu_{th} = \sqrt{\frac{\alpha}{\pi \cdot f_{lock}}} = \sqrt{\frac{k}{\pi \cdot f_{lock} \cdot \rho c_p}} \quad (2)$$

where $\alpha$ is thermal diffusity ($m^2/s$), $k$ is the thermal conductivity of the material (W/mK), $\rho$ is the density ($kg/m^3$), $c_p$ is specific heat (J/(kg·K)). For a specific material, the value of $\mu_{\text{th}}$ is determined by the lock-in-frequency. Thus, the sample is heated periodically and the temperature on the surface of the sample varies periodically as well. Due to fact that the variation of frequency is nearly equal to the lock-in frequency, the interference such as non-uniform heating, environmental reflections and surface emissivity variations can be suppressed extensively by using Fourier analysis [37]. Thus, the lock-in frequency of the excitation source should be set manually for the specific sample with different structure and characteristics. The range of lock-in frequency is usually adjusted between 0.01 Hz to dozens Hz and the carrier frequency range

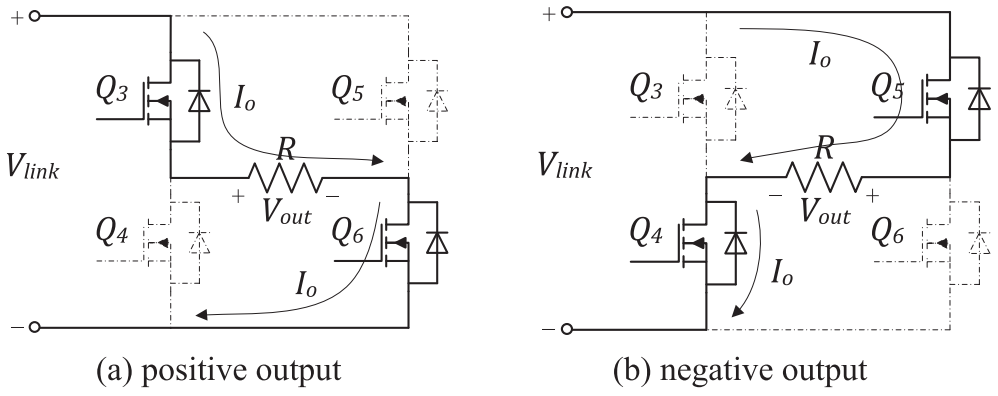


**Fig. 10.** Pulsed generation circuit (a) positive output; (b) negative output.

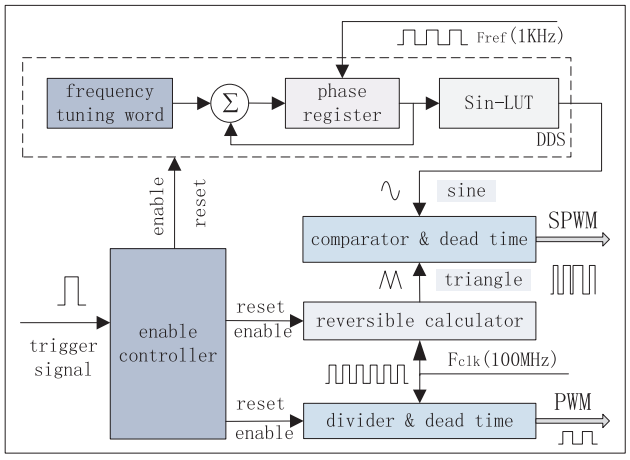


**Fig. 11.** Block diagram of the SPWM and PWM signal generation logic.

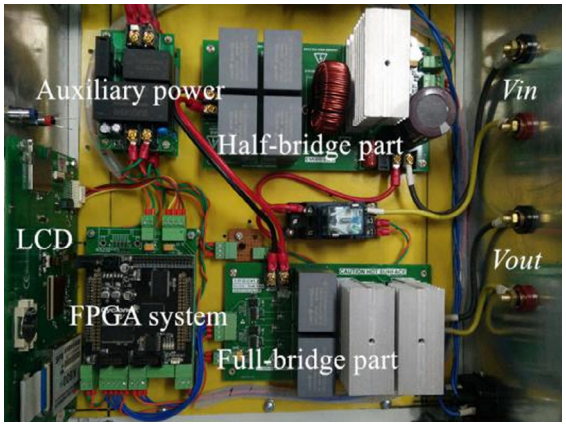


**Fig. 12.** Prototype picture.

is dozens to hundreds Hz [15,22,23,34,38].

In PT, ST, PPT mode, the pre-set current $i(t)$ can be expressed as (1) and its profile is shown in Fig. 3 [24].

$$i(t) = I_m \cdot \sin(2\pi ft) \tag{3}$$

where $I_m$ and $f$ is the current amplitude and frequency, respectively. A pulse of energy is generated by the lamps or flashes which is driven by the excitation current. The duration of the pulse is variable from μs to s depending to the thickness of material to be probed and its thermal properties. The relationship between heat propagation time $t$ and the depth $z$ of defect can be expressed as:

**Table 1**
Parameters and components of the system.

| | |
|---|---|
| Maximum input voltage | 250VDC |
| Maximum output power | 2.0 kW |
| Range of the lock-in frequency | 0.01 Hz–10 Hz |
| Switching frequency | 100 kHz |
| Range of duty cycle α | 0.1–0.9 |
| Input capacitor of sinusoidal generation circuit $C_{in1}$ | 470 μF |
| Inductor $L_f$ | 470 μH |
| Capacitor $C_f$ | 4 × 50 μF |
| Input capacitor of pulsed generation circuit $C_{in2}$ | 2 × 50 μF |
| MOSFETs $Q_1 \sim Q_6$ | IXFK64N60P |
| Gate Driver of MOSFETs | UCC27714 |
| Digital Isolators | ISO7240CF |
| FPGA chip | EP4CE15 |

**Table 2**
The measurement of the lock-in frequencies.

| Setting frequency (Hz) | Measured frequency (Hz) |
|---|---|
| 0.01 | 0.01002 |
| 0.05 | 0.05004 |
| 0.10 | 0.1001 |
| 0.50 | 0.5001 |
| 1.00 | 1.002 |
| 1.50 | 1.502 |
| 2.00 | 2.004 |
| 3.50 | 3.503 |
| 4.00 | 4.006 |
| 7.50 | 7.506 |
| 8.00 | 8.006 |
| 10.00 | 10.00 |

$$t \sim \frac{z^2}{\alpha} \tag{4}$$

where α is the material thermal diffusivity ($m^2/s$), By analyzing the variation of the surface temperature, defects can be quantitatively or qualitatively detected [37].

FMTWI and BCTWI are two recently developed techniques in thermography NDT. The profiles of the BCTWI and FMTWI are shown in Fig. 4 where they are developed and extended based on the PT mode and LT, respectively [39–41].

As discussed above, the excitation source is an important element for the optical thermography NDT system whose performance directly determines the accuracy in the detection results. Thus, with the requirements of the multi-mode optical thermography, it is necessary to design a high efficiency and lower cost excitation source.

## 3. Proposed design topology

Fig. 5 shows the block diagram of the designed excitation source

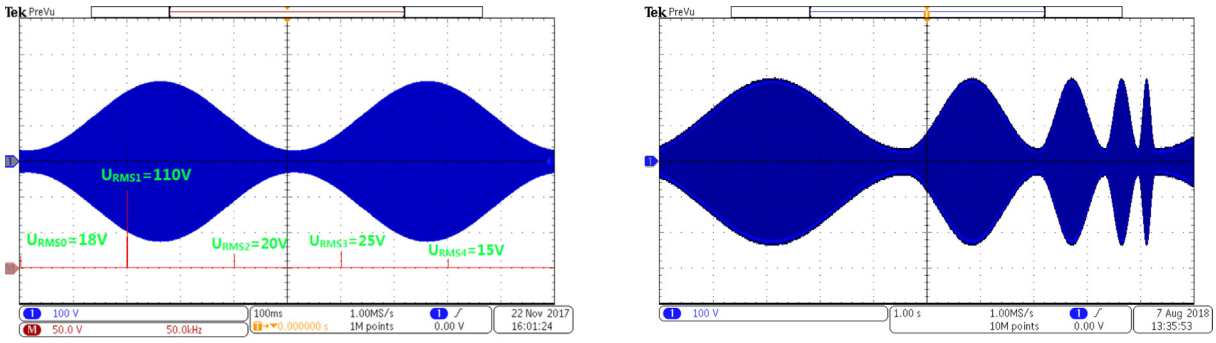


(a) LT mode (b) FMTWI mode

**Fig. 13.** Output waveform in LT mode and FMTWI mode.

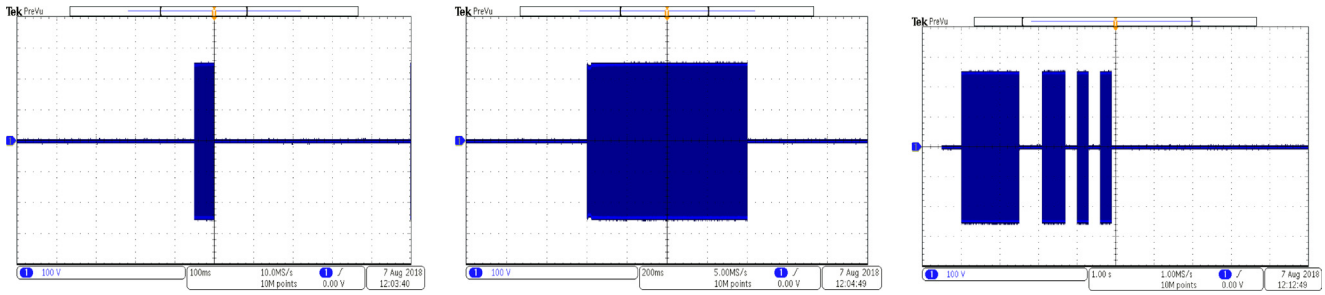


(a) PT and PPT mode (b) ST mode (c) BCTWI mode

**Fig. 14.** Output waveforms in PT, PPT, ST and BCTWI mode.

which includes five parts: Field Programmable-Gate-Array (FPGA) controller, sinusoidal generation circuit, pulsed generation circuit, drive and control circuits, interactive interface. The FPGA controller receives the configuration parameters such as operation mode, frequency, heating time, and cooling time. from the PC or touch screen through the communication interfaces and then controls the sinusoidal generation circuit and pulsed generation circuit. An ac-dc power with adjustable output voltage is prepared to supply the sinusoidal generation circuit or the pulsed generation circuit. When the AC-DC power is selected to connect with the pulsed generation circuit, the excitation source can work in PT, ST, PPT or BCTWI mode. Otherwise, the excitation source works in LT or FMTWI mode.

Fig. 6 shows the proposed design topology which mainly composes of two parts: the low frequency sinusoidal generation circuit and the pulsed generation circuit. The sinusoidal generation circuit includes a half-bridge circuit and a LC low-pass filter. The half-bridge circuit is driven by SPWM signal which can be programmed by the FPGA controller. Therefore, this structure can provide a low frequency (lock-in frequency) sinusoidal voltage ($V_{link}$) with the amplitude greater than 0 V. The pulsed generation circuit is a full-bridge chopper circuit with four power MOSFETs which are driven by square signal. This can be programmed by the FPGA controller.

When the two parts are connected in series, $V_{link}$ is modulated by the chopper circuit. Fig. 7 shows the output voltage waveform of the circuits where $V_{in}$ is set as 230VDC and the lock-in frequency is set e.g. 0.05 Hz. The circuit can work in FMTWI mode when the lock-in frequency is programmed and changed according to requirements of the FMTWI. When the pulsed generation circuit connected with the input voltage, $V_{in}$ is chopped by the full-bridge circuit and the output voltage waveform is presented in Fig. 8. As the heating and the cooling time is programmable, it can work in the PT, ST, PPT or BCTWI mode.

It should be noted that the actual output load is given by two parallel 1 kW halogen lamps which have a pure resistance characteristic. Comparing Figs. 7 and 8 with Figs. 2 and 3, the carrier signal is not a pure sinusoidal signal but rectangle signal. However, the negative effects on the defect inspection can be ignored because the carrier's fundamental component is sinusoidal and the energy of the harmonic components is small.

## 4. Operating principle

### 4.1. Sinusoidal genaration circuit

This circuit including a half-bridge circuit and a LC low-pass filter, is shown in Fig. 9 which can be considered as a buck circuit. When $Q_1$ turns on and $Q_2$ turns off, $V_{in}$ charges the inductor $L_f$ and supply to the load, $V_{o1} = V_{in}$. When $Q_1$ turns off and $Q_2$ turns on, $L_f$ discharges and the loop current freewheel through the $Q_2$ body diode, $V_{o1} = 0$ V. In the steady state, the average voltage of $V_{o1}$ is given by

$$V_{o1} = \frac{t_{on}}{t_{on} + t_{off}} V_{in} = \frac{t_{on}}{T} V_{in} = \alpha V_{in} \tag{5}$$

where $t_{on}$ is the turn-on time of $Q_1$, $t_{off}$ is the turn-off time of $Q_1$. $T$ is the switching period, $\alpha$ is the duty cycle. In this design, the switching frequency $1/T$ is set 100 kHz and the duty cycle $\alpha$ varies from 10% to 90% according to the sine mode. The circuit can work in continuous current mode (CCM) and discontinuous current mode (DCM) according to the inductor current. To achieve smaller ripple voltage, it should work in CCM while suitable inductor $L_f$ is required to be selected. Supposed $I_L$ is an average value of the inductor current $i_L$, $\Delta i_L$ is the ripple value of the inductor current $i_L$, $I_L$ and $\Delta i_L$can be expressed as

$$I_o = I_L = U_o/R \tag{6}$$

$$\Delta i_L = (V_{in} - U_o) \times \frac{\alpha T}{L} \tag{7}$$

where $\alpha = U_o/V_{in}$, $L$ is value of filter inductor $L_f$. Combining (6) and (7), the follow relation should be satisfied,

$$L \geq \frac{R \times T \times (1-\alpha)}{2} \tag{8}$$

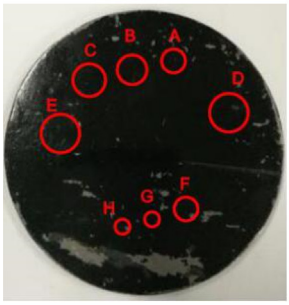


(a) Lead-steel sample

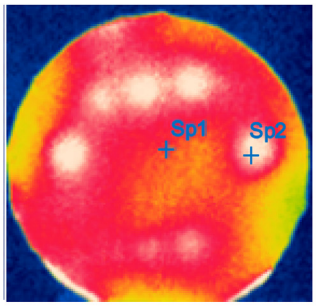


(b) Amplitude image in LT mode

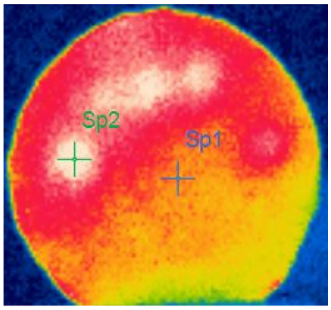


(c) Amplitude image in FTWI mode

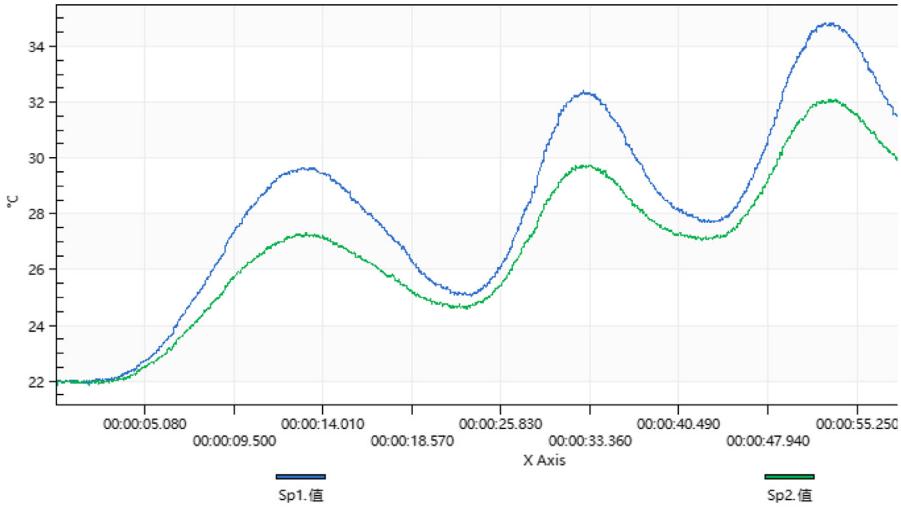


(d)Temperature evolution of the sound area and the defect area in LT mode

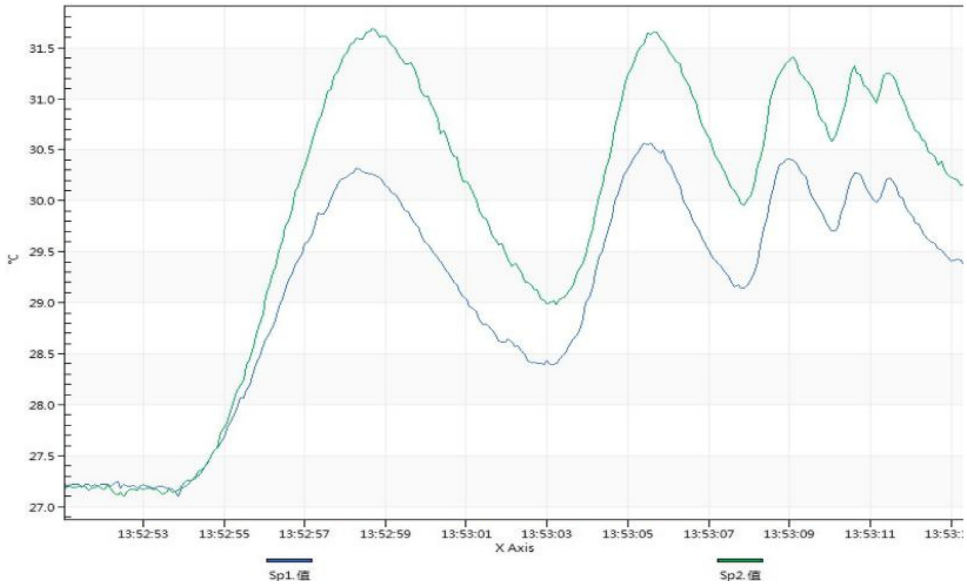


(e) Temperature evolution of the sound area and the defect area in FTWI mode

**Fig. 15.** Test sample and the detection results.

In order to satisfy (8) and consider one halogen lamp who has resistance with $R \approx 50$, switching period $T = 10\,\mu s$ and the minimum value of duty cycle is set as 10%, the minimum value of the inductor is 225 μH.

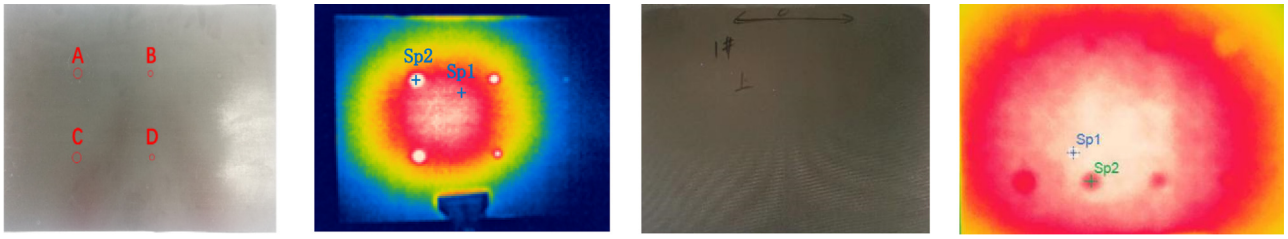


(a) Sample 'A' (b) Amplitude image of sample 'A' (c) Sample 'B' (d) Amplitude image of sample 'B'

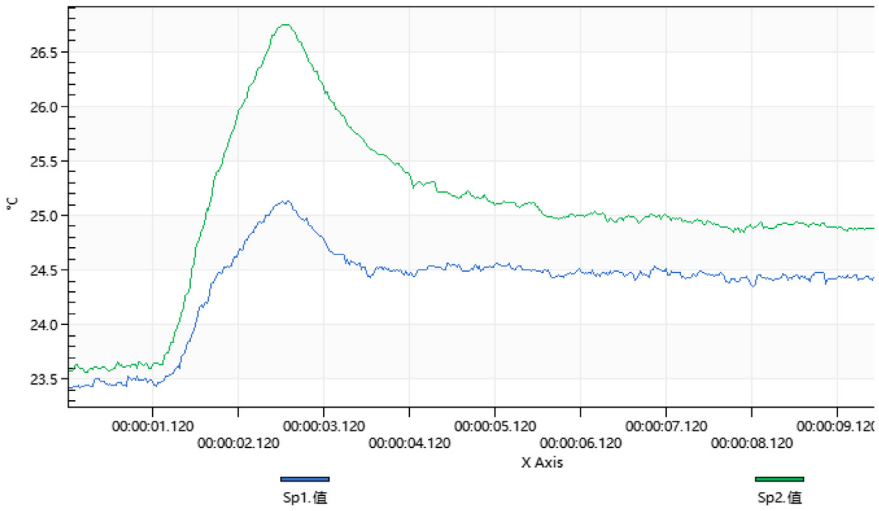


(e) Temperature evolution of sound area and defect area in PT and PPT mode

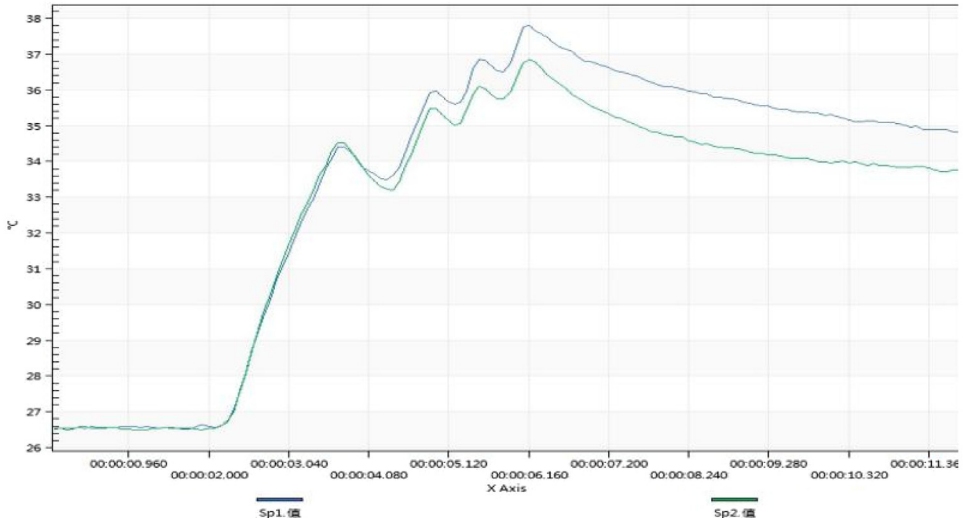


(f) Temperature evolution of sound area and defect area in BCTWI mode

**Fig. 16.** Test samples and the detection results.

### 4.2. Pulsed generation circuit

Fig. 10 shows the profile that uses a full-bridge to modulate the input the voltage $V_{in2}$ which is equal $V_{in}$ or $V_{link}$ in the different thermography modes. The switching frequency is set as 100 kHz and the duty cycle is set as 50%. In a switching period, when $Q_3$, $Q_6$ turns on and $Q_4$, $Q_5$ turns off, the output voltage on the load $R_L$ is $V_{out} = +V_{in2}$, when $Q_3$, $Q_6$ turns off and $Q_4$, $Q_5$ turns on, the output voltage on the load $R_L$ is $V_{out} = -V_{in2}$. It should be noted that $V_{link}$ varies its range from $0.1V_{in}$ to $0.9V_{in}$ that leads to a dc component of $0.1V_{in}$ and it is chopped into a series of pulses by the pulsed generation circuit in LT mode or FMTWI mode. The series of pulses constants throughout the experiment time and leads to a dc component of the increasing temperature of the sample. However, the influences of the dc component can be eliminated through the post signal processing.

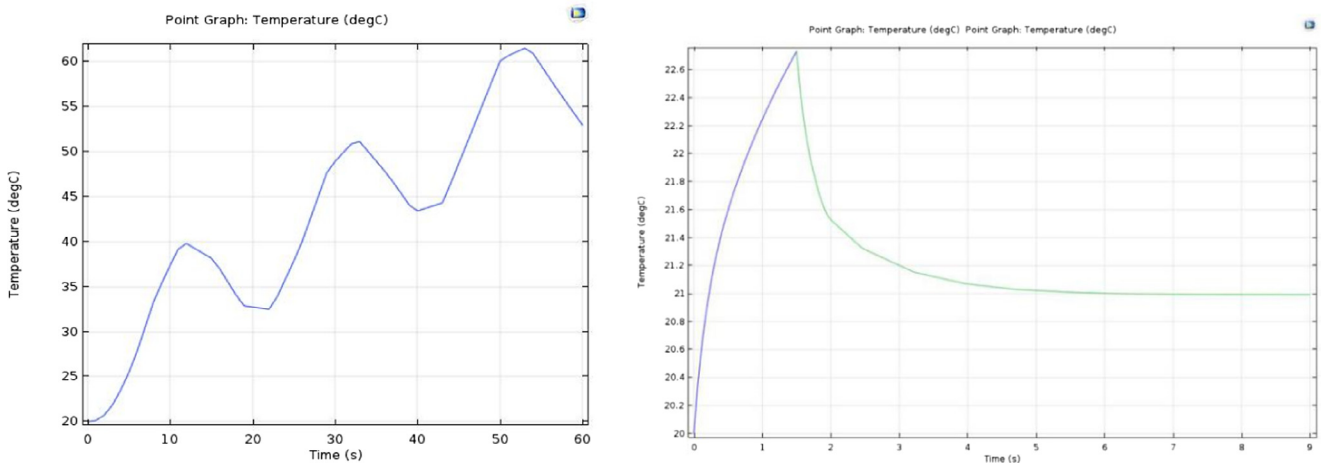


(a) Temperature evolution in LT mode (b) Temperature evolution in PT and PPT mode

**Fig. 17.** Simulation results.

### 4.3. FPGA control

Fig. 11 shows the block diagram of the SPWM and PWM signal generation logic which uses the FPGA chip. Based on the natural sampling method [42,43], the SPWM signal can be generated by comparing the discrete values of the prepared sine and triangular signals. The prepared sine signal is synthesized by using a DDS module which consists of a frequency tuning word (M) register, a phase accumulator and a sine lookup table (Sin-LUT).

The frequency control word (M) is added to the phase accumulator under the clock($F_{ref}$) control, and then the value of the phase accumulator is used as the offset address to look up the Sin-LUT to obtain the amplitude value of the sine. The frequency of the sine equals overflow frequency of the phase accumulator based on (9).

$$f_{sine} = \frac{M \cdot f_{ref}}{2^N} \tag{9}$$

where N = 33 is bits of phase accumulator, $f_{ref} = 1$ kHz, thus, the frequency resolution is $1.16415 \times 10^{-7}$ Hz. A clock $F_{clk} = 100$ MHz is divided by a divider to generate the PWM signals.

## 5. Experiment and results

The proposed topology is verified on an experimental prototype. The block diagram and parameters of the prototype are shown in Fig. 12 and Table 1, respectively. This section presents the various experimental results as obtained from the prototype.

### 5.1. Testing results of the excitation source

The excitation source was tested under the conditions that the input voltage equals 250VDC and the Resistive load of 25 Ω. The lock-in frequencies are measured under different pre-set frequencies which varies from 0.01 Hz to 10 Hz shown as Table 2, it can be seen that the maximum error is under the control within 0.2%.

The output waveform in LT mode is processed by Fourier transform where the lock-in frequency is set as 1 Hz and the result is shown in Fig. 13(a). The output includes not only the fundamental component but also the harmonic components as well as the DC component. According to (10), the average output power is approximately 535 W whereas the power of the fundamental component reaches 90.5% of the total output power, namely

$$\mathrm{P} = \frac{1}{R_L} \cdot \sum_{n=0}^{N} \frac{1}{T} \int_0^T u_n{}^2(t)dt = \frac{1}{R_L} \cdot \sum_{n=0}^{N} U_{RMSn}{}^2 dt \tag{10}$$

The output waveform in FMTWI mode is tested and shown in Fig. 13(b) which includes five pre-set lock-in frequencies: 0.1 Hz, 0.2 Hz, 0.4 Hz, 0.8 Hz and 1.6 Hz.

The output waveforms are tested where the heating time is set to 50 ms in PT, PPT mode and 800 ms in ST mode as shown in Fig. 14(a) and (b), respectively. The heating time is in accordance with set value. The output waveform in BCTWI mode is tested where the heating and cooling time are both set as 300 ms and the coded binary value is set “1111100110101” as shown in Fig. 14(c).

### 5.2. Validation of the optical thermography NDT

To validate the effectiveness of the proposed excitation source, an experiment has been done where a lead-steel sample which is bonded by industrial EP adhesive. This structure sample is quite often used in nuclear industry, the detection of inner defects of this sample is required. Several artificial defects with different diameters are used to simulate the de-bonding defects as shown in Fig. 15(a). It can be seen that the defects have been well detected when $f_{lock-in}$ is selected as 0.05 Hz in LT mode and 0.1 Hz, 0.2 Hz, 0.4 Hz, 0.8 Hz, 1.6 Hz in FMTWI mode. Fig. 15(b) and (d) shows the amplitude image in temporal domain and the diagram of temperature evolution of Sp1 point (sound area) and Sp2 point (defect area), respectively, in LT mode. Fig. 15(c) and (e) shows the amplitude image in temporal domain and the diagram of temperature evolution of Sp1 point (sound area) and Sp2 point (defect area), respectively, in FMTWI mode.

Experiments stimulated by a PT excitation current and a BCTWI excitation current, respectively, have been conducted on two different carbon fiber reinforced polymer (CFRP) samples as labeled as ‘A’ and ‘B’. Artificial defects with different diameters are used to simulate the debonding defects as shown in Fig. 16(a) and (c), respectively. In PT mode, the defects have been well detected when heating time is selected as 2000 ms. Fig. 16(b) and (e) shows the amplitude image in temporal domain and the diagram of temperature evolution of Sp1 point (sound area) and Sp2 point (defect area), respectively. In BCTWI mode, the defects have also been detected where the heating and cooling time are both set to 300 ms and the coded binary value is set “1111100110101”. Fig. 16(d) and (f) shows the amplitude image in temporal domain and the diagram of temperature evolution of Sp1 point (sound area) and Sp2 point (defect area), respectively.

The efficiency of the proposed method is validated by comparing

experimental results shown as Figs. 15(d) and 16(e) with simulation results shown as Fig. 17(a) and (b). In addition, previous studies have validated the similar characteristics [15,44,45].

## 6. Conclusion

A functional excitation source for thermography in Nondestructive Testing has been designed which can satisfy the requirements of multiple-mode excitation for optical thermography. The proposed design topology, the operating principle and the design procedure of the circuit have been investigated. A 2 kW prototype with a frequency range of 0.01 Hz–100 kHz has been designed and implemented. The performance index of the excitation source such as frequency accuracy, harmonics energy in lock-in thermography mode and accuracy of heating and cooling time in pulsed thermography have been validated. In addition, the efficiency of the proposed method has been undertaken to detect inner defects in both composite sample and lead-steel sample with bonded structure.

## References


[1] S.A. Asher, Some important considerations in the selection of a tunable UV laser excitation source, Appl. Spectrosc. 38 (2) (1984) 276–278.
[2] Stefano Sfarra, et al., Quantitative infrared thermography (IRT) and holographic interferometry (HI): nondestructive testing (NDT) for defects detection in the silicate ceramics industry, Adv. Sci. Technol. 68 (Oct) (2010) 102–107.
[3] Wolfgang Poelzleitner, Ultrasound lock-in thermography: feasibilities and limitations, Proc. SPIE 3827 (Sep) (1999) 10–15.
[4] M.H. Abdallah, S. Coulombe, J.M. Mermet, et al., An assessment of an atmospheric pressure helium microwave plasma produced by a surfatron as an excitation source in atomic emission spectroscopy, Spectrochim. Acta Part B Atom. Spectr. 37 (7) (1982) 583–592.
[5] B. Singh, S. Singh, A. Chandra, K. Al-Haddad, Comprehensive study of single-phase AC-DC power factor corrected converters with high-frequency isolation, IEEE Trans. Ind. Inf. 7 (4) (2011) 540–556.
[6] J. Rodriguez, S. Bernet, B. Wu, J.O. Pontt, S. Kouro, Multilevel voltage-source-converter topologies for industrial medium-voltage drives, IEEE Trans. Ind. Electron. 54 (6) (2007) 2930–2945.
[7] C.S. Joice, S.R. Paranjothi, V.J.S. Kumar, Digital control strategy for four quadrant operation of three phase BLDC motor with load variations, IEEE Trans. Ind. Inf. 9 (2) (2013) 974–982.
[8] J. Rodriguez, et al., State of the art of finite control set model predictive control in power electronics, IEEE Trans. Ind. Inf. 9 (2) (2013) 1003–1016.
[9] C. Buccella, C. Cecati, H. Latafat, Digital control of power converters—a survey, IEEE Trans. Ind. Inf. 8 (3) (2012) 437–447.
[10] S. Bernet, Recent developments of high power converters for industry and traction applications, IEEE Trans. Power Electron. 15 (6) (2000) 1102–1117.
[11] A. Elasser, T.P. Chow, Silicon carbide benefits and advantages for power electronics circuits and systems, Proc. IEEE 90 (6) (2002) 969–986.
[12] S. Bagavathiappan, B.B. Lahiri, T. Saravanan, John Philip, T. Jayakumar, Infrared thermography for condition monitoring - a review, Infrared Phys. Technol. 60 (5) (2013) 35–55.
[13] Y.K. Zhu, G.Y. Tian, R.S. Lu, H. Zhang, A review of optical NDT technologies, Sens. Basel 11 (8) (2011) 7773–7798.
[14] R. Yang, Y. He, Optically and non-optically excited thermography for composites: a review, Infrared Phys. Technol. 75 (March) (2016) 26–50.
[15] R. Usamentiaga, P. Venegas, J. Guerediaga, L. Vega, I. Lopez, Automatic detection of impact damage in carbon fiber composites using active thermography, Infrared Phys. Technol. 58 (5) (2013) 36–46.
[16] R. Usamentiaga, P. Venegas, J. Guerediaga, L. Vega, I. Lopez, Non-destructive inspection of drilled holes in reinforced honeycomb sandwich panels using active thermography, Infrared Phys. Technol. 55 (6) (2012) 491–498.
[17] Y.Y. Hung, Y.S. Chen, et al., Review and comparison of shearography and pulsed thermography for adhesive bond evaluation, Mater. Sci. Eng. R Rep. 64 (5–6) (May 2009) 73–112.
[18] M. Genesta, M. Martineza, N. Mradb, G. Renauda, A. Fahra, Pulsed thermography for non-destructive evaluation and damage growth monitoring of bonded repairs, Compos. Struct. 88 (1) (2009) 112–120.
[19] Zhi Zeng, Jing Zhou, Ning Tao Lichun Feng Cunlin Zhang, Absolute peak slope time based thickness measurement using pulsed thermography, Infrared Phys. Technol. 55 (2012) 200–204.
[20] Fernando Lopez, Clemente Ibarra-Castanedo, et al., Optimization of pulsed thermography inspection by partial least-squares regression, NDT E Int. 66 (2014) 128–138.
[21] Ranjit Shrestha, Wontae Kim, Evaluation of coating thickness by thermal wave imaging: a comparative study of pulsed and lock-in infrared thermography-Part I: simulation, Infrared Phys. Technol. 83 (2017) 124–131.
[22] S. Pickering, D. Almond, Matched excitation energy comparison of the pulse and lock-in thermography NDE techniques, NDT E Int. 41 (7) (2008) 501–509.
[23] A. Gleiter, C. Spiessberger, G. Busse, Lockin thermography with optical or ultrasound excitation, J. Mech. Eng. 56 (10) (2010) 619–624.
[24] J.A. Siddiqui, V. Arora, R. Mulaveesala, A. Muniyappa, Infrared thermal wave imaging for nondestructive testing of fibre reinforced polymers, Exp. Mech. 55 (7) (2015) 1239–1245.
[25] R. Mulaveesala, S. Tuli, Implementation of frequency-modulated thermal wave imaging for non-destructive sub-surface defect detection, Insight- Non-Destruct. Test. Cond. Monit. 47 (4) (2005) 206–208.
[26] V.S. Ghali, R. Mulaveesala, M. Takei, Frequency-modulated thermal wave imaging for non-destructive testing of carbon fiber-reinforced plastic materials, Meas. Sci. Technol. 22 (10) (2011) 104018.
[27] R. Mulaveesala, S. Tuli, Theory of frequency modulated thermal wave imaging for non-destructive sub-surface defect detection, Or Insight 47 (4) (2005) 206–208.
[28] R. Mulaveesala, G.S. Venkata, Coded excitation for infrared non-destructive testing of carbon fiber reinforced plastics, Rev. Sci. Instrum. 82 (5) (2011) 4902.
[29] V.S. Ghali, S.S.B. Panda, R. Mulaveesala, Barker coded thermal wave imaging for defect detection in carbon fibre-reinforced plastics, Insight- Non-Destruct. Test. Cond. Monit. 53 (11) (2011) 621–624.
[30] V. Arora, R. Mulaveesala, Pulse compression with gaussian weighted chirp modulated excitation for infrared thermal wave imaging, Prog. Electromag. Res. Lett. 44 (January) (2014) 133–137.
[31] Yunze He, Ruizhen Yang, et al., Volume or inside heating thermography using electromagnetic excitation for advanced composite materials, Int. J. Therm. Sci. 111 (2017) 41–49.
[32] R. Montanini, F. Freni, Non-destructive evaluation of thick glass fiber-reinforced composites by means of optically excited lock-in thermography, Compos. A Appl. Sci. Manuf. 43 (11) (2012) 2075–2082.
[33] J. Liu, Q. Tang, Y. Wang, The study of inspection on SiC coated carbon-carbon composite with subsurface defects by lock-in thermography, Compos. Sci. Technol. 72 (11) (2012) 1240–1250.
[34] Clemente Ibarra-Castanedo, Jean-Marc Piau, et al., Comparative study of active thermography techniques for the nondestructive evaluation of honeycomb structures, Res. Nondestr. Eval. 20 (1) (2009) 1–31.
[35] M. Vasic, OGarcía Suárez, et al., High efficiency power amplifier based on envelope elimination and restoration technique, IEEE Trans. Power Electron. 27 (1) (2011) 5–9.
[36] Concettina Buccella, Carlo Cecati, Hamed Latafat, Digital control of power converters - a survey, IEEE Trans. Ind. Inf. 8 (3) (2012) 437–447.
[37] X. Maldague, S. Marinetti, Pulse phase infrared thermography, J. Appl. Phys. 79 (5) (1996) 2694–2698.
[38] Niels Holtmann, Katia Artzt, Andreas Gleiter, Horst P. Strunk, Gerhard Busse, Iterative improvement of Lock in-thermography results [38] by temporal and spatial adaption of optical excitation, Quan. Infrar. Thermogr. J. 9 (2) (2012) 167–176.
[39] Giuseppe Silipigni, Pietro Burrascano, et al., Optimization of the pulse-compression technique applied to the infrared thermography nondestructive evaluation, NDT E Int. 87 (2017) 100–110.
[40] G. Pitarresi, Lock-in signal post-processing techniques in infra-red thermography for materials structural evaluation, Exp. Mech. 55 (2015) 667–680.
[41] Krishnendu Chatterjee, Suneet Tuli, et al., A comparison of the pulsed, lock-in and frequency modulated thermography nondestructive evaluation techniques, NDT E Int. 44 (2011) 655–667.
[42] I. Deslauriers, N. Avdiu, Boon Teck Ooi, Naturally sampled triangle carrier PWM bandwidth limit and output spectrum, IEEE Trans. Power Electron. 20 (1) (2005) 100–106.
[43] S.R. Bowes, Yen-Shin Lai, The relationship between space-vector modulation and regular-sampled PWM, IEEE Trans. Ind. Electron. 44 (5) (1997) 670–679.
[44] Liu Junyan, Liu Yang, Wang Fei, Wang Yang, Study on probability of detection (POD) determination using lock-in thermography for nondestructive inspection (NDI) of CFRP composite materials, Infrar. Phys. Technol. 70 (June) (2015) 448–456.
[45] Liu Junyan, Wang Yang, Dai Jingmin, Research on thermal wave processing of lock-in thermography based onanalyzing image sequences for NDT, Infrared Phys. Technol. 53 (June) (2010) 348–357.